Vol 15 No 10, October 2006
1009-1963/2006/15(10)/2378-07
Chinese Physics
© 2006 Chin. Phys. Soc.
and IOP Publishing Ltd

Deformation measurements of three types of Portevin–Le Chatelier bands*

Xiang Guo-Fu(项国富), Zhang Qing-Chuan(张青川)†,
Liu Hao-Wen(刘颢文), Jiang Hui-Feng(江慧丰), and Wu Xiao-Ping(伍小平)

CAS Key Laboratory of Mechanical Behavior and Design of Materials, University of Science and Technology of China, Hefei 230027, *China*

(Received 17 November 2005; revised manuscript received 2 June 2006)

In this paper a technique based on high-speed digital photography and the digital speckle correlation (DSC) method is used for the quantitative measurement of the displacement and strain fields of various Portevin–Le Chatelier (PLC) bands (types A, B, and C). The experimental results clearly show the nucleation process of a type-B band and the propagation of a type-A band. The results also reveal that there exists an elastic shrinkage deformation outside a PLC band during a large avalanche-like deformation inside the PLC band.

Keywords: Portevin–Le Chatelier (PLC) effect, digital speckle correlation (DSC) method, shear band, dynamic strain aging (DSA)
PACC: 6170Y, 8140L, 8170G

1. Introduction

An irregular plastic flow, which manifests itself as serrations (jerky flow) on the stress versus time (or strain) curves and strain staircases (discontinuous yielding) on the strain versus time curves, can be observed in many dilute alloys in various tests (including tension, compression, torsion, etc.) within a certain range of strain rate and temperature.[1−4] Spatially, this plastic instability is associated with static, hopping or propagating inhomogeneous localized bands that are usually called Portevin–Le Chatelier (PLC) deformation bands. The physical origin of the PLC effect is known to be attributed to a microstructural process denoted by dynamic strain aging (DSA): that is, the dynamic interaction between mobile dislocations and mobile solute atoms.[5,6] Mobile dislocations, which are carriers of plastic strain, move jerkily between the obstacles provided by other dislocations such as forest dislocations. Solute atoms diffuse in the stress field generated by mobile dislocations and further pin them while mobile dislocations are arrested at obstacles. So mobile dislocations need more energy provided by external stress or thermal activation to overcome the obstacles. When mobile dislocations and solute atoms have comparable mobilities, the dynamic process of aging and unpinning repeats itself. Localized deformation bands are then formed, in association with stress serrations. These bands exhibit three main types of spatial behaviours: static, hopping, and propagating, which are traditionally labelled as type-C, B, and A, respectively.[7] Type-C bands appear almost at random in the specimen without propagating, type-B bands exhibit an intermittent propagation, and type-A bands propagate continuously. The solute concentration also has significant influence on the PLC effect, which was experimentally investigated by Jiang *et al* in solution-treated Al-4%Cu alloys.[8,9]

In the past few years, several new experimental techniques, including multi-zone laser scanning extensometry,[10,11] infrared pyrometry,[12,13] laser speckle technique,[14] and so on, have been used for investigating the PLC effect. These techniques empower us to gain further insight into the spatiotemporal distribution of PLC bands. Recently, our group has proposed a novel digital speckle pattern metrology technique consisting of digital speckle pattern interferometry (DSPI) and digital speckle correlation (DSC) to study the PLC effect.[15−17] Using the technique of DSPI, not only the propagation process of PLC band during tension was monitored in real-time, but the formation, evolution and propagation of PLC band were also visualized via correlation fringe patterns.[17]

*Project supported by the National Natural Science Foundation of China (Grant Nos 1023030 and 10372098).
†E-mail: zhangqc@ustc.edu.cn

Tong *et al* [18] have recently used a technique based on high-speed digital photography and image correlation for direct whole-field strain mapping of PLC bands to measure the time-resolved strain mapping of an individual PLC band. This technique can capture the nucleation process and subsequent development of PLC bands. However, only results for a type-B band were reported in Ref.[18].

In this paper, three tensile tests with different loading speeds are performed. We use a high-speed CCD (1000 fps) to continuously record incoherent light speckle patterns of the PLC bands during the avalanche-like deformation of the PLC effect, and then obtain the whole-field axial displacement and strain distribution of the PLC bands via the digital speckle correlation method. We present here some experimentally observed spatiotemporal features of PLC bands, including the spatial distributions of the displacements and strain fields of a PLC band, the nucleation process of a type-B band, and the growths of three types PLC bands. It is also analysed and reported that there exists an elastic shrinkage deformation outside a PLC band during the formation of the PLC band in tensile tests.

The rest of this paper is organized as follows. In Section 2, we briefly introduce the experimental setting and setup. In Section 3, we give the results obtained from the experiments and their discussion. Finally some conclusions are presented in Section 4.

2. Experiment

The material of the specimens used in this study was a commercial aluminium alloy (A2017) in the form of rolled sheet of 1 mm in thickness. It was primarily a solid solution of 3.5–4.5 wt.%Cu in Al, with other alloying elements shown in Table 1. The size of specimen gauge section ($l_0 \times w_0 \times t_0$) was 55mm×20mm×1mm. For eliminating the effect of internal stress, the specimens were annealed at 773 K for 4 hours before loading tests. The average grain size was about 40μm after heat treatment. The loading direction was along the rolling direction.

Table 1. Contents of A2017 commercial alloy.

Element	Cu	Fe	Mn	Mg	Cr	Si	Zn	Ti	Other	Al
wt. percent/%	3.5–4.5	0.7	0.4–1.0	0.4–0.8	0.1	0.2–0.8	0.25	0.15	0.35	the rest

Figure 1 is a schematic illustration of the experimental setup. The specimen was fully clamped at both ends and stretched under displacement control by a special tensile machine at a constant crosshead speed. On the right-hand side in Fig.1 is a system of DSPI, which was used for monitoring the formation and propagation of PLC bands in real-time, and on the left-hand side is a high-speed collection system. The detailed description of the DSPI system can be found in Refs.[15,17]. The high-speed CCD was post-triggered when a PLC band, which could be observed from the real-time DSPI monitor system, occurred in the view field of the high-speed CCD, then a total number of 2048 frames incoherent light speckle patterns prior to the triggering point were captured. Each of the recorded 8-bit grey scale digital images had a size of 512×512 pixels with a spatial resolution of 47μm per pixels. These digital images were cropped into 384×512 pixels which matched the central part of specimen gauge section before analysis with the DSC method. The in-plane displacement fields reported here were originally obtained by image analysis between two digital speckle images via the DSC method, and then locally fitted by moving least-square (MLS) surface fitting[19] with influence radius 100 pixels. The strain fields were calculated under the small deformation assumption. The errors in local in-plane displacement and strain measurements were estimated to be 0.01 pixels and 100×10^{-6}, respectively, for a macroscopically homogeneous field.

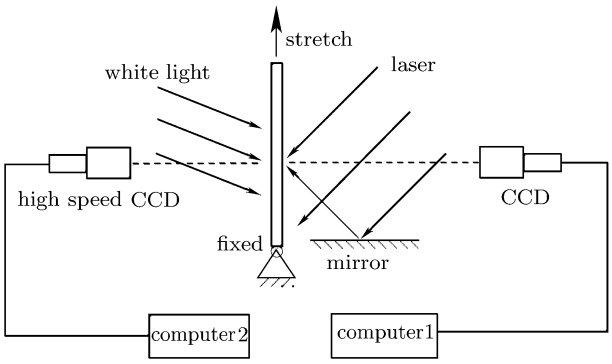


Fig.1. A schematic illustration of the experimental setup.

3. Results and discussion

The tests were performed at room temperature at three different loading speeds (v_0): 2 mm/min,

0.8 mm/min and 0.1 mm/min, corresponding to nominal strain rates ($\dot{\varepsilon} = v_0/l_0$): $6.1 \times 10^{-4}s^{-1}, 2.4 \times 10^{-4}s^{-1}$ and $3.0 \times 10^{-5}s^{-1}$, respectively. These nominal strain rates fall into the respective strain rate domain where type-A, B, C bands occur in Al–Cu alloys.

Figure 2 shows the different type loading curves recorded at various strain rates. These repeated serrated stress *vs* time curves are an identification of the PLC effect. In order to clearly distinguish among them, we remove the respective linear elastic parts from these curves. The inset in Fig.2 is a close-up view, showing the typical serrated plastic flows. From these overall curves, we find that the amplitude of serrations, which is a macroscopic representation of the intensity of DSA, gradually increases with the increase of strain. This is possibly due to gradual increase in densities of mobile and immobile dislocations with the increase of strain.[20] As a result, the intensity of the interaction between mobile dislocations and solutes becomes stronger and stronger.

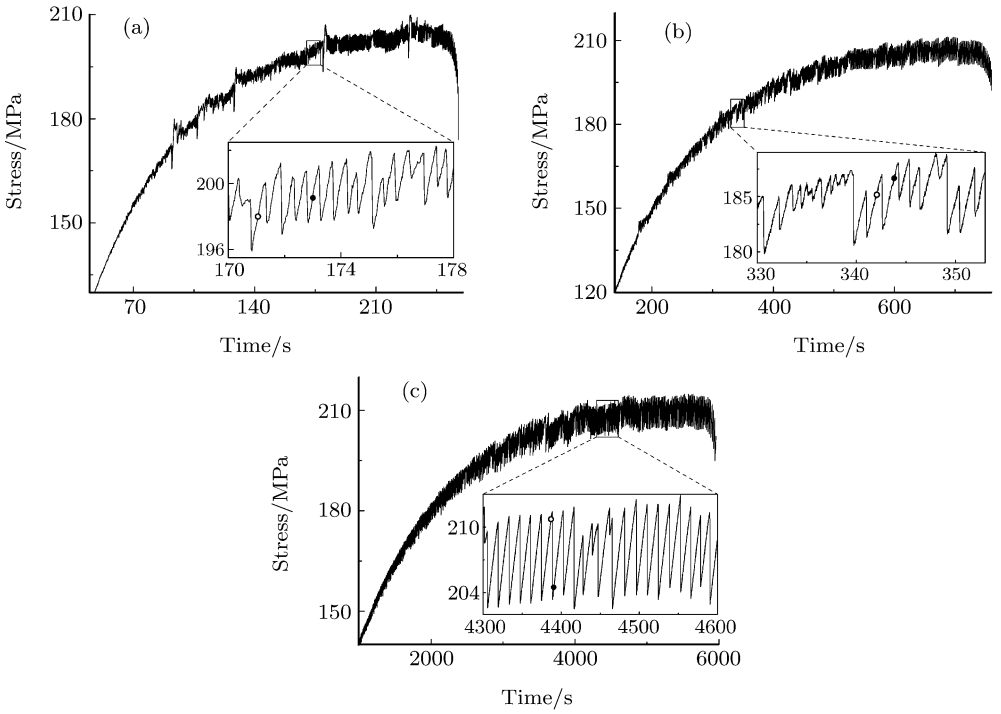


Fig.2. Three types of serrated stresses versus time of the PLC effect in Al–Cu alloy. The solid circles (•) on the zoom-in curves indicate the respective post-triggering points in three tension tests and the open circles (○) are corresponding to the start of image capture of PLC band. (a) Type-A with nominal strain rate $\dot{\varepsilon}_0 = 6.1{\times}10^{-4}s^{-1}$, (b) type-B with nominal strain rate $\dot{\varepsilon}_0 = 2.4{\times}10^{-4}s^{-1}$, (c) type-C with nominal strain rate $\dot{\varepsilon}_0 = 3.0{\times}10^{-5}s^{-1}$.

Serration patterns on the deformation curves, traditionally designated as type-A, type-B and type-C serrations, are easily recognized from the inset in Fig.2. Type-A serrations seem to be irregular. Type-B serrations are a series of serration patterns which consist of several small serrations subsequently followed by a big stress drop. Type-C serrations are more orderly and more periodic than the other two types. For three specimens having almost the same ductility (about 18%), it is obvious that the amplitude of serrations decreases with the increase of strain rate by comparing the amplitudes at the same strain level on the overall loading curves in Fig.2.

Using the technique of DSPI, we are able to observe the growth and propagation of the PLC bands in real time from fringe patterns.[17] Four successive fringe patterns each containing an inclined narrow 'white band' in the middle of these images, which is a PLC band propagating downward, are shown in Fig.3. The fringes in the fringe patterns represent the contours of axial in-plane displacement of the specimen surface.

Figure 4(a) is an incoherent light speckle pattern captured by the high-speed CCD and Fig.4(b) is the displacement vector field of a PLC band calculated using the DSC method. For the convenience of image analysis, the coordinate system has its origin at the left top corner of the image, x-axis pointing to the right and y-axis oriented along the downward direction that is opposite to the direction of the loading. We can find from Fig.4(b) that the centre of the band holds still, and the upper and lower parts shear in opposite directions.

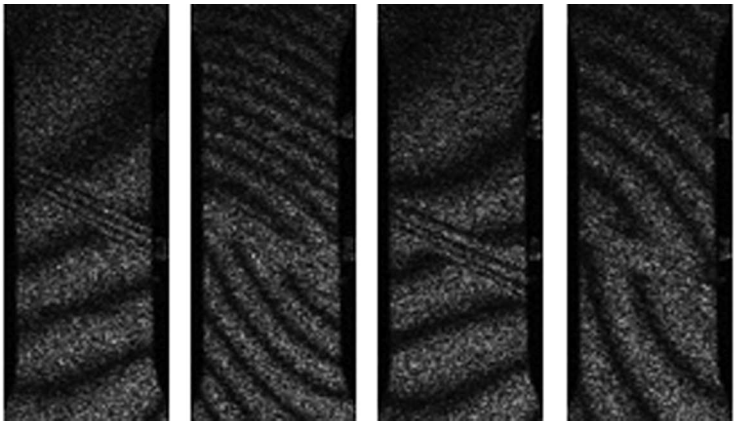


Fig.3. Four successive fringe patterns of a propagating band obtained using the technique of DSPI.

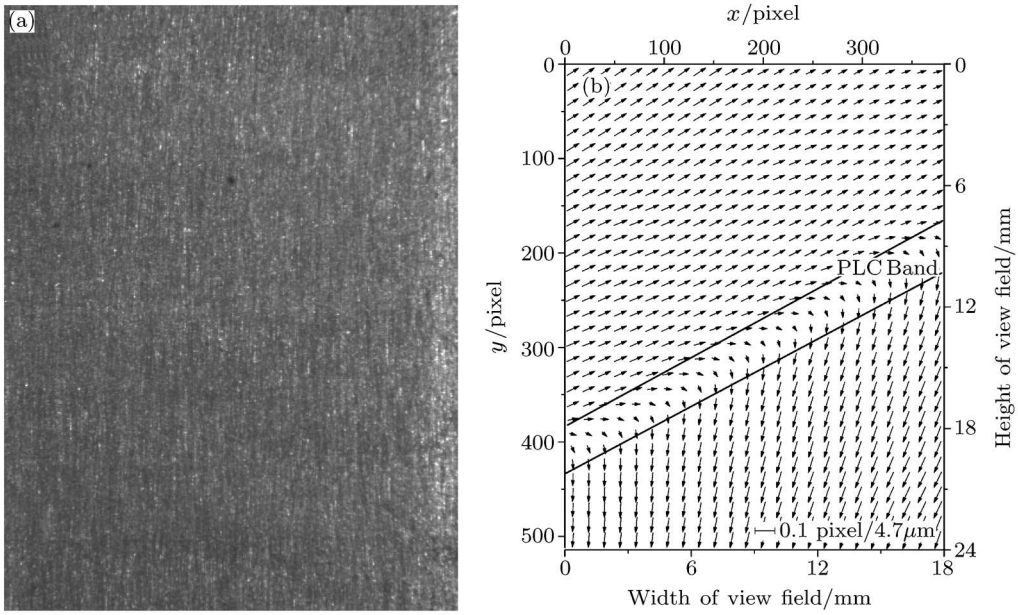


Fig.4. (a) An incoherent light speckle pattern. (b) The displacement vector field of a PLC band calculated using the DSC method.

Figures 5 and 6 show the spatial distributions of axial displacements and the corresponding axial true strains associated with the nucleation and growth of a type-B PLC band. Each of the spatial distributions is obtained through the DSC of the first captured image, with the image recorded at the capture time Δt relative to the time when the first image was captured. The first figures in Figs.5 and 6 respectively show the axial displacement field and the axial true strain field just at the beginning of initiation of a type-B PLC band on one of the edges of the specimen. At this time, the average axial displacement and axial true strain are still very small (close to zero) and almost homogeneous. 2 ms later, the deformation band transversely grows into the bulk at an angle (consistent with the resulting band orientation) with respect to the tensile axis but is still not a complete band (Figs.5(b) and 6(b). As seen from Fig. 6(b), the peak strain level decreases from one edge to another along the band orientation. Then another 2 ms later, the type-B band becomes a complete PLC band transversely across the specimen associated with an avalanche style of deformation which is up to 0.2% in under 2 ms (Figs.5(c) and 6(c)). Hence, the deformation inside the band gradually increases (Figs.5(d) and 6(d)).

Moreover, the deformation bands are much localized (only about 2–3 mm in width) and are inclined to the specimen axis at a well-defined angle $\varphi \approx \pm 30^\circ (\pm 2^\circ)$ with respect to the transverse direction. On the other hand, as seen from Fig.6, the deformation outside the PLC band is almost homogeneous and close to zero during the formation of PLC band.

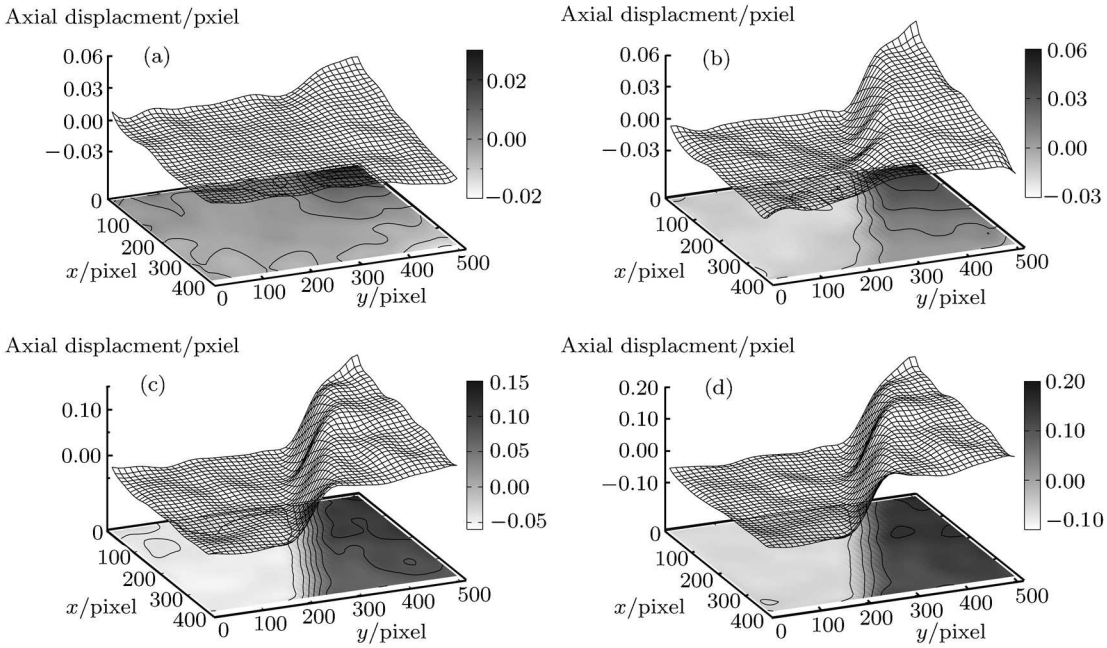


Fig.5. Spatial distributions of displacement of type-B PLC band, showing the nucleation process of type-B band. (a) $\Delta t = 666$ ms, (b) $\Delta t = 668$ ms, (c) $\Delta t = 670$ ms, (d) $\Delta t = 674$ ms. The time Δt used here is relative to the time when the first image was captured, which is also used below unless otherwise stated.

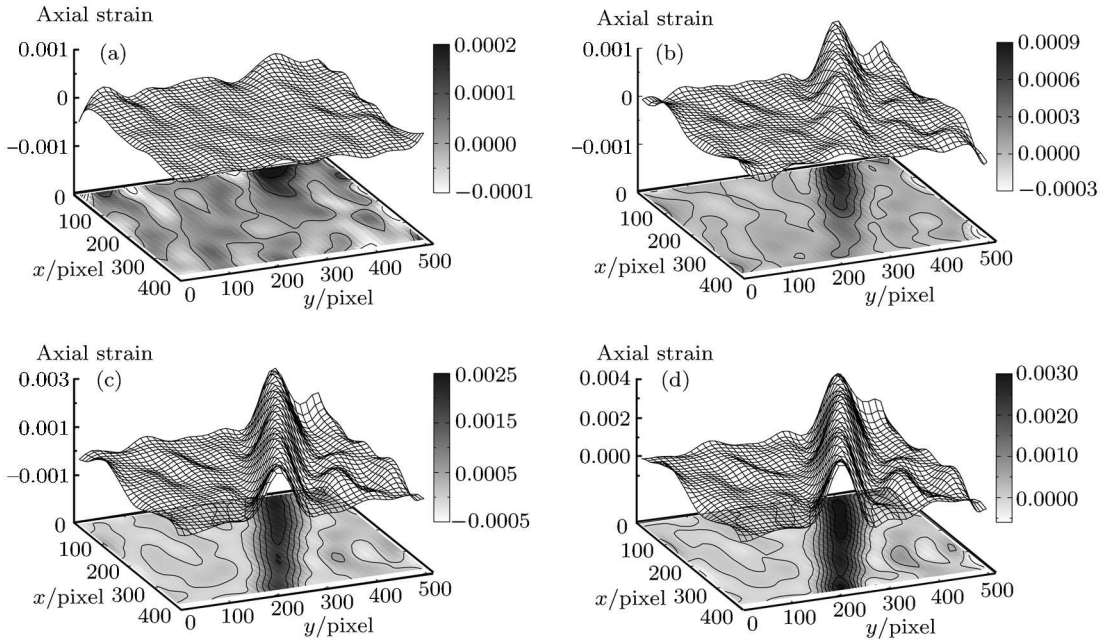


Fig.6. Spatial distributions of axial strains of type-B PLC band, clearly showing the nucleation process of type-B band.

Temporal variations in axial profile of strain distribution are plotted in Fig.7 in order to determine the growth and motion of the PLC band. The selected profile corresponds to a column located at the centre of the specimen, and the choice of this column does not alter the appearance of the distribution.

At each selected time, the strain profile takes the form of a bell-like peak except for embryo band. It is clearly seen that there appears a shift of the type-A band strain distribution along the tensile direction during the capture time. Actually, there are four bands intermittently occurring and continually propagating along the tensile direction. The avalanche-like deformation occurs only within a few milliseconds, i.e. 280–284 ms, 806–810 ms, 1322–1326 ms and 1928–1932 ms respectively. However, no major shifts of the type-B and C bands are detected. Each avalanche-like deformation corresponds to a stress drop (see the

serrations between the trigger points in Fig.2).

From these strain profiles, we can estimate that the maximum strain rate $\dot{\varepsilon}_{\rm m}$ during the formation of PLC band is nearly up to 1 s^{-1}, which is at least three orders of magnitude larger than the nominal strain rate $\dot{\varepsilon}_0$. But the band width $w_{\rm B}$ is only a few millimetres (2–3 mm), which is only one order of magnitude less than the length of gauge section (l_0 = 55 mm).

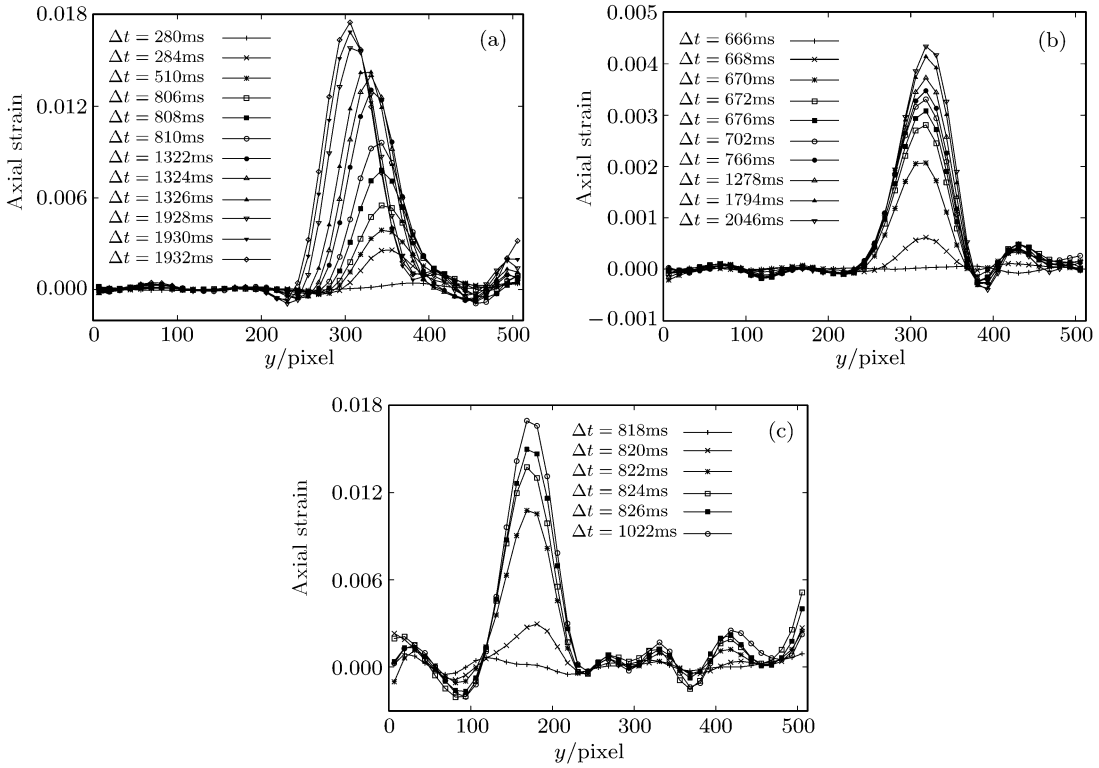


Fig.7. Axial strain distributions of three types of PLC bands along the central line of the specimen at selected times. (a) type-A PLC band, (b) type-B PLC band, (c) type-C PLC band.

Therefore, $\dot{\varepsilon}_{\rm m}\tau w_{\rm B}$ (about 5–7 μm) is about two orders of magnitude larger than $\dot{\varepsilon}\tau l_0$(about 0.03–0.07 μm), where τ(about 2 ms) is the time duration of the avalanche-like relaxation. In other words, the magnitude of the plastic deformation inside the PLC band is much larger than the displacement of the crosshead during an avalanche-like deformation. Hence, there exists an elastic shrinkage deformation outside the PLC band, which makes the specimen satisfy the compatibility of displacement. Actually, this is also confirmed from Fig.4(b), which is the displacement vector field computed from two speckle patterns before and after the avalanche-like deformations. With a specimen fixed at the bottom and stretched up on a tensile machine, all the displacement vectors should point to the loading direction under the condition of homogeneous deformation, but the result in Fig.4(b) shows that the lower part shifts in the opposite direction of the loading. This indicates that the lower part of specimen suffers a shrinkage: that is to say, there exists an elastic unloading process outside the PLC band during the avalanche-like deformation. The upper part also experiences a shrinkage, which can be verified by shrinkage fringes.[17] According to our tests, we find that the elastic shrinkage deformation occurs only during a large avalanche-like deformation, usually for the type-B or type-C band. It is not obvious for the type-A band, because the high loading speed results in a shrinkage smaller than either shrinkage of other two types of PLC bands.

4. Conclusions

In this article, the spatial distributions of axial displacements and axial true strains of PLC band are quantitatively presented by the DSC method. The experimental results clearly show that the nucleation process of type-B PLC band is associated with the initiation of an embryo band at a lateral specimen surface through subsequent transversal growth into the bulk at an angle with respect to the tensile axis. The type-A deformation band propagates continually, while type-B and C bands remain stationary. The

avalanche-like deformation inside the PLC band occurs within only a few milliseconds and the maximum strain rate inside the PLC band is at least three orders of magnitude larger than the nominal strain rate. Elastic shrinkage deformation may occur outside a PLC band during a large avalanche-like deformation inside the PLC band.

References

[1] Portevin A and Le Chatelier F 1923 *Comp. Rend. Acad. Sci.* **176** 507

[2] McReynolds A W 1949 *Trans. Am. Inst. Min. Metall. Pet. Eng.* **185** 32

[3] Bell J F 1984 *Mechanics of Solids* Vol. I (New York: Springer) p 41, 649

[4] Picu R C, Vincze G, Qzturk F, Gracio J J, Barlat F and Maniatty 2005 *Mater. Sci. Eng.* A **390** 334

[5] Cottrell A H 1953 *Dislocations and Plastic Flow in Crystals* (London: Oxford University Press)

[6] McCormick P G 1972 *Acta Metall.* **20** 351

[7] Chihab K, Estrin Y, Kubin L P and Vergnol J 1987 *Scr. Metall.* **21** 203

[8] Jiang H F, Zhang Q C, Xu Y H and Wu X P 2006 *Acta Phys. Sin.* **55** in press (in Chinese)

[9] Jiang H F, Zhang Q C, Sun L and Wu X P 2006 *Chin. Phys.* **15** 1051

[10] Ziegenbein A, Hahner P and Neuhauser H 2000 *Comp. Mater. Sci.* **19** 27

[11] Neuhauser H, Klose F B, Hagemann F, Weidenmuller J, Derke H and Hahner P 2004 *J. Alloys Compounds* **378** 13

[12] Ranc N and Wagner D 2005 *Mater. Sci. Eng.* A **394** 87

[13] Louche H, Vacher P and Arrieux R 2005 *Mater. Sci. Eng.* A **404** 188

[14] Shabadi R, Kumar S, Roven H J and Dwarakadasa E S 2004 *Mater. Sci. Eng.* A **364** 140

[15] Jiang H F, Zhang Q C, Jiang Z Y, Chen Z J and Wu X P 2005 *Chin. Phys. Lett.* **22** 99

[16] Jiang Z Y, Zhang Q C, Jiang H F, Chen Z J and Wu X P 2005 *Mater. Sci. Eng.* A **403** 154

[17] Zhang Q C, Jiang Z Y, Jiang H F, Chen Z J and Wu X P 2005 *Int. J. Plast.* **21** 2150

[18] Tong W, Tao H, Zhang N and Hector Jr LG 2005 *Scr. Mater.* **53** 87

[19] Zeng Q H and Lu D T 2004 *J. Eng. Graph.* **25** 84 (in Chinese)

[20] Estrin Y and Kubin L P 1986 *Acta Metall.* **34** 2455